

# MagicHand: Context-Aware Dexterous Grasping Using an Anthropomorphic Robotic Hand

Hui Li, Jindong Tan and Hongsheng He

**Abstract**—Understanding of characteristics of objects such as fragility, rigidity, texture and dimensions facilitates and innovates robotic grasping. In this paper, we propose a context-aware anthropomorphic robotic hand (MagicHand) grasping system which is able to gather various information about its target object and generate grasping strategies based on the perceived information. In this work, NIR spectra of target objects are perceived to recognize materials on a molecular level and RGB-D images are collected to estimate dimensions of the objects. We selected six most used grasping poses and our system is able to decide the most suitable grasp strategies based on the characteristics of an object. Through multiple experiments, the performance of the MagicHand system is demonstrated.

**Index Terms**—Dexterous Grasping, Characteristics of Objects Recognition, NIR Spectrum, RGB-D Images

## I. INTRODUCTION

Context-aware systems are designed to collect useful information from their environments and adapt their behaviors based on the information [1]. This idea is widely used in robot cooperation [2], patients assistant, object tracking [6], swarm robotics system [7] etc. Dexterous manipulation is able to aid the robot to accomplish complicate grasp tasks, especially for those tasks which require precise manipulation and dangerous or infeasible to humans, such as planetary exploration, underwater salvage, and objects retrieval under dangerous environments. It is a complex decision-making process that depends on the task to be performed and the physical characteristics of the object such as fragility, rigidity, texture, shape and dimensions.

Near-infrared spectroscopy (NIRS) is increasingly becoming one of the most efficient analytical tool [8], [9], [10]. Near-infrared spectrum is the near-infrared region (780 nm to 2500 nm) of electromagnetic spectrum. In the near-infrared range, the molar absorption is very little so that the NIR can penetrate much further into a sample. This advantage makes NIRS very useful in recognizing materials with little or no sample preparation. A SCiO sensor is a palm-sized molecular analyzer which is able to measure NIR spectrum

Hui is with the Department of Electrical Engineering and Computer Science, Wichita State University, Wichita, KS, 67260, USA, e-mail: hxl14@shockers.wichita.edu.

Jindong tan is with the Department of Mechanical, Aerospace, and Biomedical Engineering, University of Tennessee, Knoxville, TN, 37996, USA, e-mail: tan@utk.edu.

Hongsheng He is with the Department of Electrical Engineering and Computer Science, Wichita State University, Wichita, KS, 67260, USA, e-mail: hongsheng.he@wichita.edu.

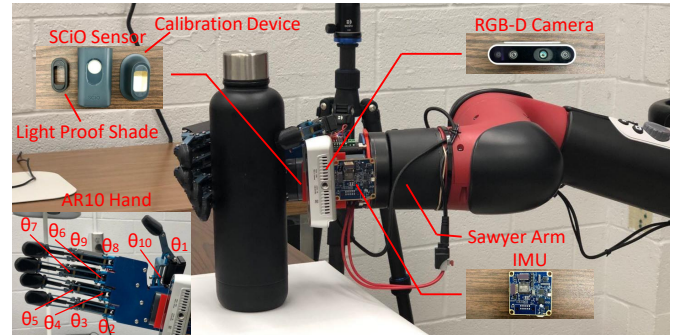


Fig. 1. MagicHand Platform: An AR10 robotic hand is attached to a Sawyer robotic arm to interact with the outside environment. A SCiO sensor and an RGB-D camera were assembled on the wrist of the AR10 hand to collect useful information for the system.

of an object. The spectrum collection process takes only several seconds which makes the SCiO sensor very suitable for online material recognition.

RGB-D technique is widely used in 3D reconstruction, object recognition and 3D mapping. A new 3D object recognition method using RGB-D data explored by Qi [11] has greatly reduced the time cost for localizing the target object and improved data processing efficiency. Endres utilized an RGB-D camera on small domestic robots to generate high accurate 3D maps [12]. All these applications greatly improved the robot perception of the environments in real time.

In this paper, we present a context aware grasping system named MagicHand as shown in Fig. 1. This platform is designed to achieve dexterous grasping on target objects based on the information collected by the sensors in the platform, the performance of this system was demonstrated through multiple experiments.

## II. MAGICHAND SYSTEM OVERVIEW

The MagicHand platform is an object oriented, context-aware dexterous grasping system which is capable of generating a proper grasping strategy to manipulate a target objects based on the information perceived by the sensors. In this platform, an AR10 anthropomorphic robotic hand and a Sawyer robotic arm are attached together to interact with target objects. A SCiO sensor is used to recognize the materials/characteristics of objects and an RGB-D camera (Intel Realsense D435 depth camera) is employed to estimate

dimensions of objects. Instead of using a fixed camera, we assemble an RGB-D camera on the wrist of the robotic hand so that the camera can move with the hand. In this way, RGB-D images can be collected from different views, thus further improve the understanding of the object. In addition, an algorithm is developed to collect the desired information and determine grasping strategies based on the acquired information.

### III. MATERIAL PERCEPTION

We established two datasets to train the algorithm. The first dataset is called MLP dataset which contains 15936 ideal spectra of six materials from 540 samples. We call these spectra ideal spectra since all spectra were collected in an ideal environment with a light proof shade where the noises and errors can be neglected. The other dataset is called AE dataset, an example of the AE dataset is shown in Fig. 2. The AE dataset contains 1080 pairs of NIR spectra  $(SI, SP)_k$  where  $SI$  is an idea spectrum collected from a sample in lab environment and  $SP$  is a practical spectrum gathered from the same location of the sample by the MagicHand platform. Before feeding the spectra into the network, the raw data was pre-processed with standard normal variate (SNV) to improve the performance of the whole system.

#### A. NIR Spectrum Denoising and Reconstruction

NIR spectra can be classified perfectly in an ideal environment where noises and errors can be neglected. However, in practical, noises are not avoidable and may lead to a low classification accuracy. In this work, we trained a complex structure of autoencoders (shown in Fig. 3) with the AE dataset to reduce noises and improve performance of our algorithm.

In the algorithm,  $x_i$  is the  $i^{th}$  feature in a pre-processed ideal spectrum where  $1 \leq i \leq 331$  corresponds 331 features in an NIR spectrum.  $\tilde{x}_i$  is the corresponding practical features of  $x_i$  in AE database.  $\tilde{x}_i$  was then encoded by algorithm and five most important features were extracted. The algorithm would then try to decode the extracted features and generate reconstructed spectrum  $\hat{x}_i$  by minimizing the reconstruction error.

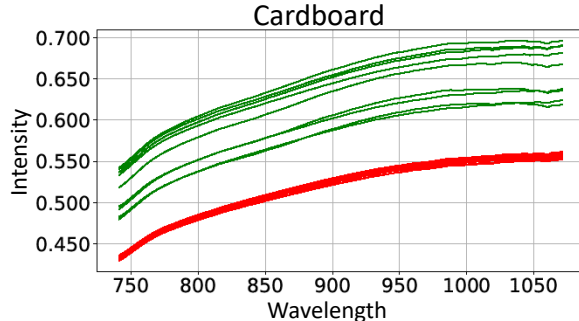


Fig. 2. Example of ideal spectra (red) and practical spectra (green).

#### B. Characteristics Classification

With NIR spectra, material type of an object can be recognized and then characteristics such as fragility, rigidity, and texture are mapped to the perceived material.

1) *Material Classification*: A MLP deep neural network was developed specifically for our MLP dataset. Rectified Linear Units (ReLU) were used as activation functions in the first five layers. In the first layer, 331 neurons were used to match the number of features of NIR spectrum. In the next four layers,  $2^{10}$ ,  $2^9$ ,  $2^8$  and  $2^5$  neurons were employed to further calibrate the model. The output layer contains six neurons and Softmax functions were used to classify the data. The network was trained with 70% of data and achieved an overall 99.96% accuracy.

TABLE I  
MATERIAL TO CHARACTERISTICS MAPPING LIST

Materials	Fragility	Rigidity	Texture
Wood	sturdy	rigid	rough
Glass	medium	rigid	smooth
Plastic	medium	soft	smooth
Ceramic	sturdy	rigid	slippery
Cardboard	medium	rigid	rough
Stainless Steel	sturdy	rigid	grippy

2) *Characteristics Mapping*: Once the material of an object was recognized, characteristics are mapped to the perceived material through a material-to-characteristics table (Table I). This table was established based on an existing dataset [13]. Three characteristics including fragility, rigidity and texture were extracted and assigned to each corresponding material. This information would then be used to learn grasping strategies.

### IV. OBJECT DIMENSION MEASUREMENT

There were two challenges in the dimension estimation process. The first one was to separate the object from its background and the other one was to find orthogonal directions of the object to measure the dimensions of that object precisely.

#### A. Object detection in point cloud

An RGB-D point cloud/image might contain multiple objects, separating the target object from the others was necessary for dimension estimation. By utilizing an existing 2D detector named Yolo3 [14], we successfully detected the target object in an RGB image. In the next step, we reconstructed the target in 3D using Open3D [15], [16], [17] with a sequence of RGB-D images of that object. Given depth information  $D$  and intrinsic matrix  $I$  which described the relationship between a stream's 2D and 3D

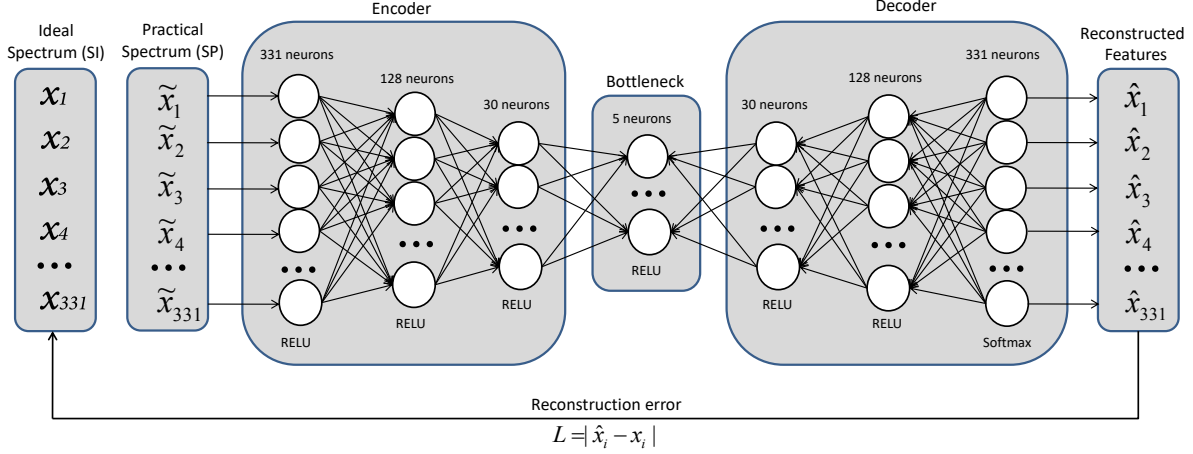


Fig. 3. Structure of autoencoder for noise reduction

coordinate systems, a pixel  $(px, py)$  in an RGB image could be deprojected to a point  $(x, y, z)$  in 3D point cloud with

$$\begin{aligned} x &= (px - ppy)D/fy \\ y &= (py - ppx)D/fx \\ z &= D \\ I &= \begin{bmatrix} fx & 0 & ppx \\ 0 & fy & ppy \\ 0 & 0 & 1 \end{bmatrix} \end{aligned} \quad (1)$$

where  $fx$  and  $fy$  are focal length of the image,  $ppx$  and  $ppy$  are coordinates of center of projection, these information can be collected directly from the RGB-D sensor. To extract the target object in 3D point cloud, all pixels that belong to the target object detected by the 2D detector were deprojected to points in 3D space and any point within this region was cropped from the point cloud to establish a 3D model of the target object.

### B. Axis Dimension for Grasping

While an object is placed in front of a camera, the object could be placed in different positions (distance), angles or even on a slop. All these factors may bring difficulties in estimating dimensions of the object. We need to find dimensions of an object in orthogonal directions which will not be affected by the way the object is observed. To solve this problem, we first found the centroid point  $C = (\bar{X}, \bar{Y}, \bar{Z})$  where  $\bar{X}$ ,  $\bar{Y}$  and  $\bar{Z}$  were the average value of Cartesian coordinates of all points in a point cloud. Then we clustered the point cloud into  $m$  groups and found centroid points  $c_j$  of those groups as shown in 2 where  $x_i$  was the  $i^{th}$  point in points cloud and  $g_i$  represented the group that contained  $x_i$ .

$$\begin{aligned} g_i &= \arg \min_j ||x_i - c_j||^2 \\ c_j &= \frac{\sum_{i=1}^n 1\{g_i = j\} x_i}{\sum_{i=1}^n 1\{g_i = j\}} \quad j \in [0, 1, 2 \dots m] \end{aligned} \quad (2)$$

For the third step, euclidean distance were calculated between  $C$  and  $c_i$  and find  $p_{near}$  and  $p_{far}$  by

$$\begin{aligned} p_{near} &= \arg \min ||C - c_j|| \\ p_{far} &= \arg \max ||C - c_j|| \end{aligned} \quad (3)$$

Now we could determine a plane  $h$  with  $C$ ,  $p_{near}$  and  $p_{far}$  and thus two vectors in  $h$ :  $a = p_{near} - C$  and  $b = p_{far} - C$ . And we calculated a vector  $c$  which was orthogonal to plane  $h$  through centroid point  $C$  with equation

$$c = ||a|| ||b|| \sin(\theta) \lambda \quad (4)$$

where  $||a||$  and  $||b||$  were magnitude of vector  $a$  and  $b$ ,  $\theta$  was the angle between  $a$  and  $b$  and  $\lambda$  was a unit vector perpendicular to the plane  $h$ . Since the longest distance from centroid points to a point in an object was usually the diagonal, the angle between  $a$  and  $b$  might not be a right angle. In this case, we needed to find a new vector  $b'$  which was perpendicular to both vector  $a$  and  $c$  through centroid point  $C$ . The lengths of vector  $a$ ,  $b'$  and  $c$  could be determined by existing realsense API.

### V. GRASPING STRATEGIES GENERATION

Human grasping choices are based on task and properties of target objects [18] and they trend to cluster over a large set of objects [19], [20]. To simplify the problem [21], we defined six grasping descriptions  $d_i$  as shown in Fig. 4 where  $d_i$  is a ten dimensional vector of joint angles of AR10 hand  $\theta_i$ . These grasping descriptions are suitable for a wide range of objects. For example, Power Circular Grasp, Power Heavy Wrap Grasp, Power Prismatic Grasp and Power Thin Grasp are able to provide secure and stable grasping for sturdy, rigid or rough objects while Precision Circular Grasp and Precision Prismatic Grasp are more suitable for objects that require dexterous or sensitive manipulations. With these pre-defined grasp choices, we can simplified the problem as

$$G_i = \beta d_i$$

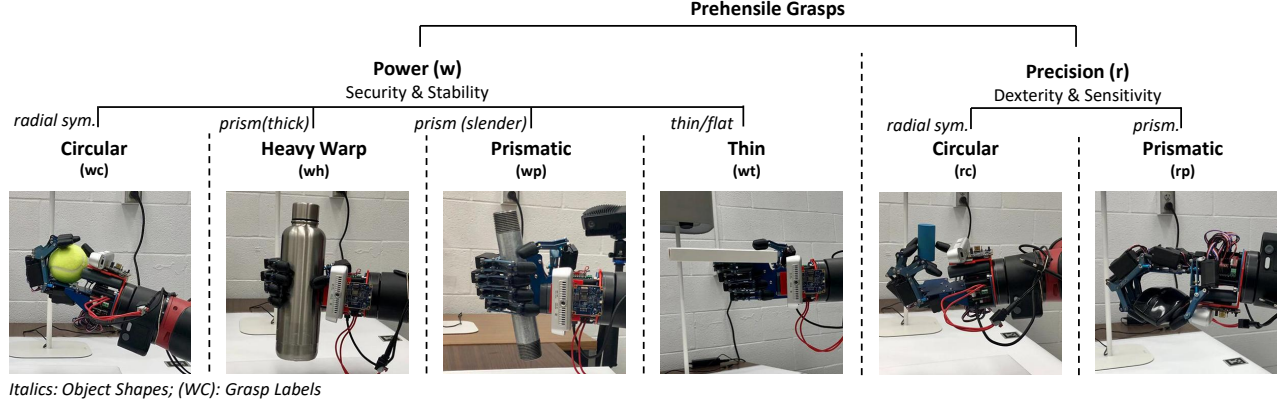


Fig. 4. Pre-defined grasping descriptions

where  $G_i$  is learned grasping postures,  $\beta$  is a scalar that related to the size of an object and  $d_i$  is the pre-defined grasping choices. With the problem simplified, we now need to generate proper grasping strategies based on the information gathered by the MagicHand system, that is, map features of objects  $F$  to grasp  $G_i$ ,

$$F = [l, h, w, m, s, r, mt] \rightarrow G_i$$

features  $l$ ,  $h$  and  $w$  are dimensions along orthogonal directions of target objects and  $l \geq h \geq w$ . Features  $m$ ,  $s$ ,  $r$  and  $mt$  are stand for mass ( $g$ ), shape, rigidity and material type of the target object. We tested the performance of the context-aware grasping system using grasp selection neural network model in [13], [22]. The model considers learning grasp type and grasp dimension are independent from each other and includes two separate neural networks in Fig. 5. The network contains a hidden layer with 75 neurons which employ ReLU as activation functions and an output layer with Softmax as its activation function. Also grid search is used

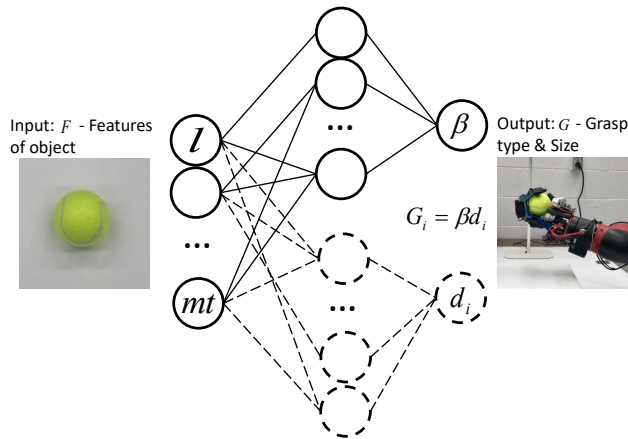


Fig. 5. Neural Network Classification Model for grasp pose selection and grasp size determination. Two neural networks were employed, one was used for grasp type  $d_i$  selection and the other was able to decide grasp size  $\beta$ . Input for both networks are perceived features of target object  $F$ .

to tune  $L_2$  and  $\alpha$  is set to 3.6. The cross-validation score for both grasp types and grasp dimensions are around 80%.

## VI. EXPERIMENTS

Ten grasping experiments were performed to test the performance of the MagicHand system. For each trial, the system first localized the object and the hand navigated around the object to collect RGB-D data to reconstruct a 3D model of that object, this process took about 90 seconds. Then the hand put the SCiO sensor as close to the object as possible to gather NIR spectrum which would be used for material detection and characteristics mapping. Based on both NIR spectrum and 3D model of the target object, a grasping strategy was generated and executed to grasp the object. This step took about 30 seconds and the overall process took approximately 120 seconds.

### A. Materials Classification

Near-infrared spectra of six types of materials including ceramic, stainless steel, wood, cardboard, plastic and glass

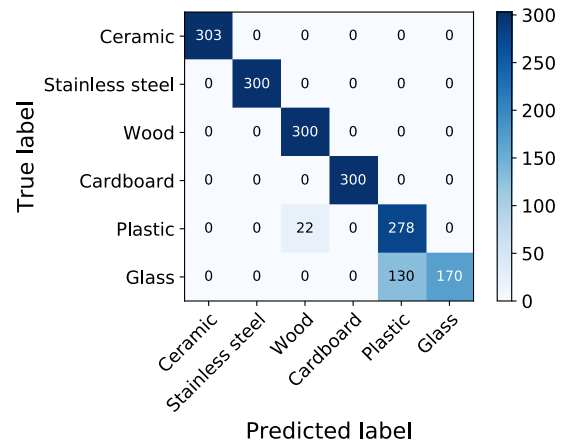


Fig. 6. Confusion matrix for MLP network.



were collected in this work. All these materials covered a major majority of daily objects. A total of 54 different daily used objects were selected. This material/object selection pattern would expand the universality of our datasets. Two NIR datasets were established to train the material/feature detection algorithm. MLP dataset was collected to train a MLP network for material recognition while AE dataset is used to train our autoencoder to reduce noise in practical spectra.

1) *Material Recognition Results:* We extracted the spectra of one object from each material in the MLP dataset. This part of the data (1803 scans) was separated and used as the validation set to evaluate the final performance of the classifier. The rest of data was divided into training and testing set. 70% of the data was used to train the network and 30% of the data was used as the testing set. We tuned the hyper-parameters as follows: 64 batch size, 50 epochs and ADAM optimizer with 0.0001 learning rate. The MLP network achieved a 99.64% test accuracy and 1.95% test loss. The pre-extracted validation data (1803 scans) which was completely new to the algorithm were tested with the algorithm. A total 1609 correct predictions were achieved by the algorithm as shown in Fig. 6. The results show that our algorithm had a very high performance in recognizing ceramic, stainless steel, wood and card board while had a less performance on predicting plastic and glass objects due to the characteristics of those two materials. The autoencoder was trained with the AE dataset to reduce noises and errors.

To evaluate the performance of the whole material/features recognition system, we selected another twelve new objects which fall into the six material categories and collected NIR spectra of those objects in a practical environment (temperature  $63^{\circ}F$  and less light intensity). 60 spectra were collected (five scans per object) by the MagicHand platform and the classifying results achieved 60/60. Although the prediction result was perfect, there were two reasons that might lead to this result. Firstly, the autoencoder greatly reduced noises from practical spectrum. Secondly, there were only sixty testing samples in this experiment. As the number of testing samples increases, the accuracy is expected to decrease.

TABLE II  
DIMENSIONS OF TARGET OBJECT

Objects	Measured Dimensions (mm)	Estimated Dimensions (mm)
1	151 x 73 x 73	149.9 x 74.0 x 73.0
2	152 x 38 x 38	154.2 x 41.4 x 35.3
3	244 x 71 x 71	246.3 x 69.6 x 71.2
4	149 x 44 x 44	152.6 x 46.4 x 41.3
5	154 x 77 x 26	152.4 x 75.4 x 27.6
6	65 x 65 x 65	65.9 x 67.6 x 68.0
7	166 x 82 x 19	163.5 x 81.2 x 19.1
8	114 x 29 x 29	112.7 x 28.5 x 30.2
9	59 x 29 x 29	61.2 x 29.7 x 27.8
10	71 x 71 x 71	74.6 x 72.9 x 71.5

## B. Dimension Estimation

Before grasping, the robot arm took a sequence of RGB-D images around that object to reconstruct the 3D model of the target object, dimensions were then estimated based on the 3D model by our algorithm. The detailed dimensions are shown in table II. In the table, measured dimensions indicate the real world dimensions collected with a 0-150 mm digital caliper and a steel tape. The estimated dimensions were estimated by our algorithm and the errors were less than 4 mm.

## C. Object Grasping

With the characteristics and dimensions of target objects, we tested the grasp strategy generation system on ten objects. If the robot hand could hold/lift an object for 10 seconds without dropping it, we counted the grasp as a success. The experiment results showed 8 out 10 successes on picking up the objects as shown in Fig. 7. There were two failures in the robot trials, the first failure was a plastic tube (object 8), the system gave a mismatch on grasp selection which led to a fail grasp. The other failure was on a wood block (object 9), the system gave a proper grasp choice, but the robotic hand slipped due to inadequate friction.

## VII. CONCLUSION

In this paper, we presented a context-aware dexterous grasping system called MagicHand. This system is able to collect NIR spectrum from objects to achieve material recognition with an accuracy of 99.64%. The dimensions of object is estimated based on the 3D model of target object and robot trials was performed on 10 objects with 8/10 successes. From the experiment results, we conclude that the MagicHand system is efficient in perceiving useful information about its target object and generate proper grasping strategy base on perceived information in different working environments.

## REFERENCES

- [1] B. Schilit, N. Adams, and R. Want, "Context-aware computing applications," in *wmcas*. IEEE, 1999, pp. 85–90.
- [2] E. Tuci, R. Groß, V. Trianni, F. Mondada, M. Bonani, and M. Dorigo, "Cooperation through self-assembly in multi-robot systems," *ACM Transactions on Autonomous and Adaptive Systems (TAAS)*, vol. 1, no. 2, pp. 115–150, 2006.
- [3] W.-H. Mou, M.-F. Chang, C.-K. Liao, Y.-H. Hsu, S.-H. Tseng, and L.-C. Fu, "Context-aware assisted interactive robotic walker for parkinson's disease patients," in *2012 IEEE/RSJ International Conference on Intelligent Robots and Systems*. IEEE, 2012, pp. 329–334.
- [4] G. Lacey and S. MacNamara, "Context-aware shared control of a robot mobility aid for the elderly blind," *The International Journal of Robotics Research*, vol. 19, no. 11, pp. 1054–1065, 2000.
- [5] J. George, D. Kluger, T. Davis, S. Wendelken, E. Okorokova, Q. He, C. Duncan, D. Hutchinson, Z. Thumser, D. Beckler *et al.*, "Biomimetic sensory feedback through peripheral nerve stimulation improves dexterous use of a bionic hand," *Science Robotics*, vol. 4, no. 32, p. eaax2352, 2019.
- [6] M. Mamei and F. Zambonelli, "Pervasive pheromone-based interaction with rfid tags," *ACM Transactions on Autonomous and Adaptive Systems (TAAS)*, vol. 2, no. 2, p. 4, 2007.

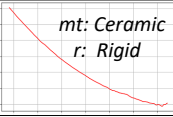

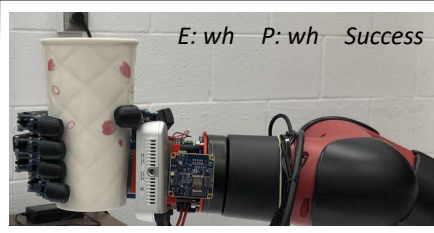
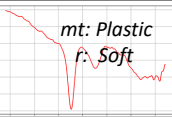
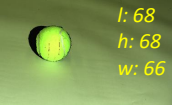
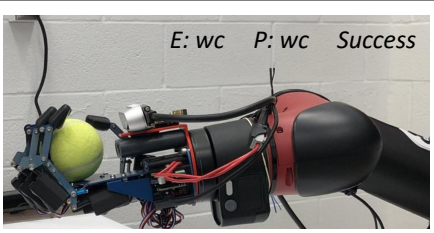
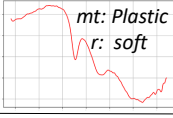
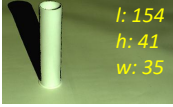
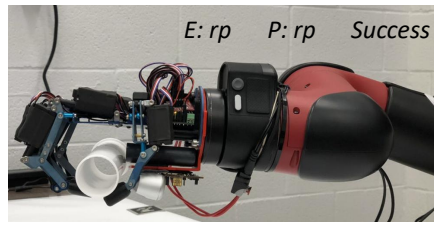
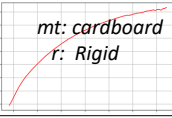

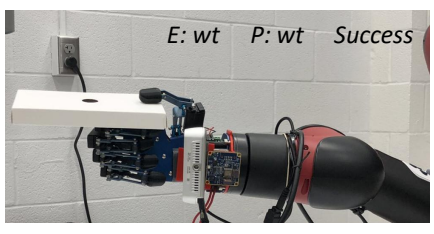
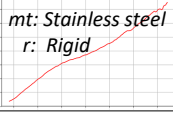

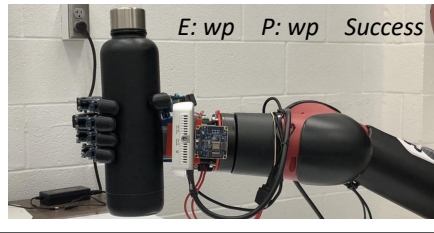
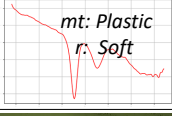

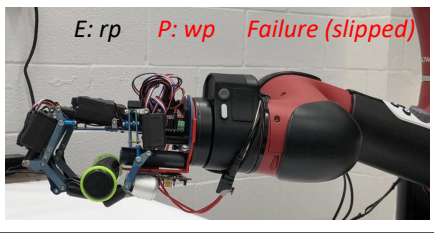
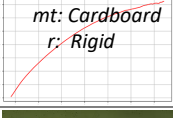
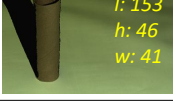
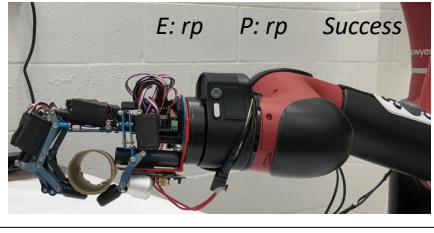
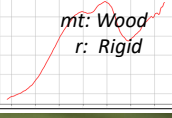

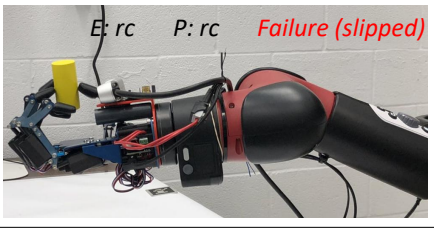
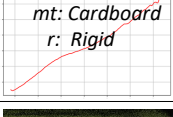
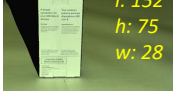
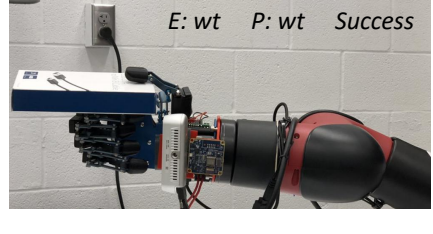
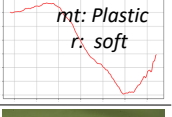

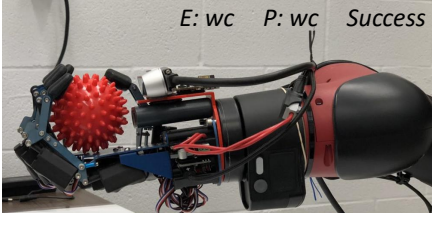
Input	Robot Trial	Input	Robot Trial
 <p>mt: Ceramic r: Rigid</p>  <p>l: 150 h: 74 w: 73</p>	 <p>E: wh P: wh Success</p>	 <p>mt: Plastic r: Soft</p>  <p>l: 68 h: 68 w: 66</p>	 <p>E: wc P: wc Success</p>
 <p>mt: Plastic r: soft</p>  <p>l: 154 h: 41 w: 35</p>	 <p>E: rp P: rp Success</p>	 <p>mt: cardboard r: Rigid</p>  <p>l: 164 h: 81 w: 19</p>	 <p>E: wt P: wt Success</p>
 <p>mt: Stainless steel r: Rigid</p>  <p>l: 246 h: 71 w: 70</p>	 <p>E: wp P: wp Success</p>	 <p>mt: Plastic r: Soft</p>  <p>l: 113 h: 29 w: 30</p>	 <p>E: rp P: wp Failure (slipped)</p>
 <p>mt: Cardboard r: Rigid</p>  <p>l: 153 h: 46 w: 41</p>	 <p>E: rp P: rp Success</p>	 <p>mt: Wood r: Rigid</p>  <p>l: 61 h: 30 w: 28</p>	 <p>E: rc P: rc Failure (slipped)</p>
 <p>mt: Cardboard r: Rigid</p>  <p>l: 152 h: 75 w: 28</p>	 <p>E: wt P: wt Success</p>	 <p>mt: Plastic r: soft</p>  <p>l: 75 h: 73 w: 72</p>	 <p>E: wc P: wc Success</p>

Fig. 7. Robot grasp experiments with 10 objects. E stands for expected grasp type while P is predicted grasp type. Failure indicates the robot was not able to pick up the object and P in red means predicted grasp type does not match expected grasp type.

- [7] Y. Khaluf and M. Dorigo, "Modeling robot swarms using integrals of birth-death processes," *ACM Transactions on Autonomous and Adaptive Systems (TAAS)*, vol. 11, no. 2, p. 8, 2016.
- [8] J. Li, W. Huang, C. Zhao, and B. Zhang, "A comparative study for the quantitative determination of soluble solids content, ph and firmness of pears by vis/nir spectroscopy," *Journal of Food Engineering*, vol. 116, no. 2, pp. 324–332, 2013.
- [9] B. K. Wilson, H. Kaur, E. L. Allan, A. Lozama, and D. Bell, "A new handheld device for the detection of falsified medicines: demonstration on falsified artemisinin-based therapies from the field," *The American journal of tropical medicine and hygiene*, vol. 96, no. 5, pp. 1117–1123, 2017.
- [10] R. M. Balabin, R. Z. Safieva, and E. I. Lomakina, "Comparison of linear and nonlinear calibration models based on near infrared (nir) spectroscopy data for gasoline properties prediction," *Chemometrics and intelligent laboratory systems*, vol. 88, no. 2, pp. 183–188, 2007.
- [11] C. R. Qi, W. Liu, C. Wu, H. Su, and L. J. Guibas, "Frustum pointnets for 3d object detection from rgb-d data," *arXiv preprint arXiv:1711.08488*, 2017.
- [12] F. Endres, J. Hess, J. Sturm, D. Cremers, and W. Burgard, "3-d mapping with an rgb-d camera," *IEEE transactions on robotics*, vol. 30, no. 1, pp. 177–187, 2014.
- [13] B. Rao, "Learning robotic grasping strategy based on natural-language object descriptions," 2018.
- [14] J. Redmon and A. Farhadi, "Yolov3: An incremental improvement," *arXiv preprint arXiv:1804.02767*, 2018.
- [15] Q.-Y. Zhou, J. Park, and V. Koltun, "Open3D: A modern library for 3D data processing," *arXiv:1801.09847*, 2018.
- [16] S. Choi, Q.-Y. Zhou, and V. Koltun, "Robust reconstruction of indoor scenes," in *Proceedings of the IEEE Conference on Computer Vision*

- and *Pattern Recognition*, 2015, pp. 5556–5565.
- [17] J. Park, Q.-Y. Zhou, and V. Koltun, “Colored point cloud registration revisited,” in *Proceedings of the IEEE International Conference on Computer Vision*, 2017, pp. 143–152.
  - [18] R. S. Johansson and J. R. Flanagan, “Coding and use of tactile signals from the fingertips in object manipulation tasks,” *Nature Reviews Neuroscience*, vol. 10, no. 5, p. 345, 2009.
  - [19] T. Feix, J. Romero, H.-B. Schmiedmayer, A. M. Dollar, and D. Kragic, “The grasp taxonomy of human grasp types,” *IEEE Transactions on Human-Machine Systems*, vol. 46, no. 1, pp. 66–77, 2016.
  - [20] M. Santello, M. Flanders, and J. F. Soechting, “Postural hand synergies for tool use,” *Journal of Neuroscience*, vol. 18, no. 23, pp. 10 105–10 115, 1998.
  - [21] M. R. Cutkosky *et al.*, “On grasp choice, grasp models, and the design of hands for manufacturing tasks,” *IEEE Transactions on robotics and automation*, vol. 5, no. 3, pp. 269–279, 1989.
  - [22] F. Pedregosa, G. Varoquaux, A. Gramfort, V. Michel, B. Thirion, O. Grisel, M. Blondel, P. Prettenhofer, R. Weiss, V. Dubourg *et al.*, “Scikit-learn: Machine learning in python,” *Journal of machine learning research*, vol. 12, no. Oct, pp. 2825–2830, 2011.